Submitted to Physics of Fluids

LBL-3266
Preprint c.1

SOME PROPERTIES OF DEEP WATER SOLITONS

Bruce I. Cohen, Kenneth M. Watson, and Bruce J. West

June 6, 1975

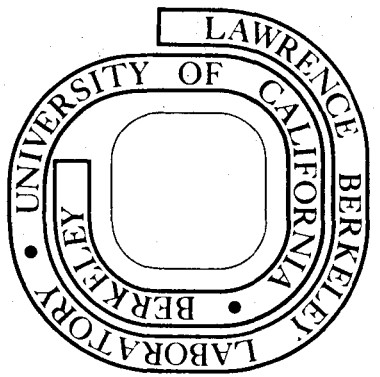

Prepared for the U. S. Energy Research and
Development Administration under Contract W-7405-ENG-48

DISCLAIMER

SOME PROPERTIES OF DEEP WATER SOLITONS*

Bruce I. Cohen and Kenneth M. Watson

Department of Physics and Lawrence Berkeley Laboratory
University of California, Berkeley, California 94720

and

Bruce J. West

Physical Dynamics, Inc.
P. O. Box 1069
Berkeley, California

June 6, 1975

ABSTRACT

Envelope solitons for surface waves in deep water are studied using the coupled equation for the Fourier amplitudes of the surface displacement. Comparison is made with some wave-tank experiments of Feir. A linear stability analysis is made for an imposed transverse ripple. A slowly growing instability is found at wavelengths comparable to, or longer than, the length of the soliton. A slowly developing instability is found also for a soliton propagating through a train of waves of wavelength appreciably smaller than that of the soliton. A soliton propagating through a train of waves with wavelength much larger than that of the soliton exhibits gross distortion due to the orbital fluid velocity of the wavetrain. This distortion is to some extent reversible, as the soliton tends to "recover" when the wavetrain is damped to zero amplitude. Some comments are given concerning the statistics of a wave field containing solitons.

I. INTRODUCTION

The hydrodynamic equations describing the gravity wave field on the surface of an inviscid, irrotational fluid also may be written so as to describe the envelope function for a packet of surface waves. The propagation of a symmetric wavepacket of deep water waves was studied by Lighthill.[1] In his analysis nonlinear interactions led to the development of a nonsymmetric shape and a peaking of the packet envelope function.

Benney and Newell[2] have observed that certain waveforms have a persistent shape due to the balancing of nonlinear and dispersive effects. Chu and Mei[3] have used a nonlinear WKB method, with the inclusion of dispersion, to study some steady and some nonsteady wavetrains. Similar studies have been made by Davey[4] and by Lake and Yuen[5] who used the average Lagrangian method of Whitham[6] to derive the nonlinear Schrödinger equation. This equation describes the envelope function of a narrow bandwidth train of deep water waves. Among the solutions of this equation which were studied, are those for envelope solitons.[7] Zakharov and Shabat[8] have shown that these solitons are stable when interacting with other wavetrains described by the same nonlinear Schrödinger equation. It is to be emphasized that these solitons (and other persistent waveforms) are one-dimensional wavetrains.

Experimental studies of soliton-like wavetrains propagating in wave tanks have been reported by Feir[9] and by Lake and Yuen[5]. The observed properties of these wave systems seem to be consistent with theoretical expectaions.[3,5]

The above approaches[3-7] assume a slowly varying amplitude for the wavetrain. Another approach to the investigation of surface wave

interactions is to decompose the wave amplitude into Fourier modes. The interactions then appear as nonlinear couplings of the linear mode amplitudes.[10,11,12] This technique was used by West, Watson and Thomson,[13] who made a numerical analysis of the coupled mode equations. In this analysis a tendency for "bumps" in the envelope of a wavetrain to grow was noted by the authors. Indeed, unless care was taken to avoid such "bumps" when the initial conditions were selected, the growth of these tended to obscure the other phenomena being studied.

The purpose of this paper is to investigate soliton propagation using the coupled mode equations of Ref. (13). In Section II the nonlinear Schrödinger equation will be obtained as an approximation to the coupled mode equations. Solutions for envelope solitons and the Benjamin-Feir[14] instability criteria will be noted for subsequent reference.

Some numerical examples of the propagation and distortion of solitons will be given in Section III, where the calculated results are compared with observations from wavetanks.

Soliton stability is studied in Section IV. It is shown that a periodic modulation parallel to the wavecrests causes a rather slowly growing instability. It is also shown that even in the one-dimensional case that the envelope soliton appears to be unstable upon encountering a second wavetrain of substantially different wave numbers than those of which the soliton is constructed. This does not violate the conclusions of Zakharov and Shabat,[8] since the two wavetrains of substantially different frequencies each satisfy different nonlinear Schrödinger equations.

Section V considers some statistical aspects of a wave field containing solitons.

II. RELATION OF THE MODE COUPLING EQUATIONS TO THE NONLINEAR SCHRÖDINGER EQUATION

Following Ref. (13), we let the x-y plane of a rectangular coordinate system coincide with the undisturbed surface of the fluid, the depth of which is considered to be much larger than the wavelength of those surface waves studied. A two dimensional vector in the surface plane is indicated as $\underset{\sim}{x} = (x,y)$. The wave height at position $\underset{\sim}{x}$ and time t is $\zeta(\underset{\sim}{x},t)$. The corresponding velocity potential at $z = 0$ is $\phi_s(\underset{\sim}{x},t)$.[15] A complex amplitude $Z(\underset{\sim}{x},t)$ is introduced as

$$Z(x,t) = V_x^{-1}\,\phi_s - i\zeta\,. \tag{1}$$

Here

$$V_x = g^{\frac{1}{2}}/(-\nabla_s^2)^{\frac{1}{4}}\,,$$

is the phase velocity operator and ∇_s the two-dimensional gradient operator acting on the coordinates (x,y).

We suppose our "ocean" to be rectangular and of area Σ. A discrete Fourier representation of Z can then be written in the form

$$Z(\underset{\sim}{x},t) = \sum_{\underset{\sim}{k}} a_{\underset{\sim}{k}}(t)\,\exp(i\,\underset{\sim}{k}\cdot\underset{\sim}{x}). \tag{2}$$

Equations satisfied by the $a_{\underset{\sim}{k}}$'s were obtained in Ref. (13) to be of the form

$$\dot{a}_{\underset{\sim}{k}} + i\omega_k\, a_{\underset{\sim}{k}} = \sum_{\underset{\sim}{\ell},\underset{\sim}{p}} \delta_{\underset{\sim}{k}-\underset{\sim}{\ell}-\underset{\sim}{p}}\; C^{\underset{\sim}{k}}_{\underset{\sim}{\ell}\underset{\sim}{p}}\; a_{\underset{\sim}{\ell}}\, a_{\underset{\sim}{p}} + \sum_{\underset{\sim}{\ell},\underset{\sim}{p}} \delta_{\underset{\sim}{k}+\underset{\sim}{p}-\underset{\sim}{\ell}}\; C^{\underset{\sim}{k}\underset{\sim}{p}}_{\underset{\sim}{\ell}}\; a_{\underset{\sim}{\ell}} a^*_{\underset{\sim}{p}}$$

$$+\; i \sum_{\underset{\sim}{\ell},\underset{\sim}{p},\underset{\sim}{n}} \delta_{\underset{\sim}{k}+\underset{\sim}{n}-\underset{\sim}{\ell}-\underset{\sim}{p}}\; C^{\underset{\sim}{k}\underset{\sim}{n}}_{\underset{\sim}{\ell}\underset{\sim}{p}}\; a_{\underset{\sim}{\ell}}\, a_{\underset{\sim}{p}}\, a^*_{\underset{\sim}{n}} + \mathcal{O}(a^4) \tag{3}$$

in the absence of viscous damping and wave generation due to wind.

Here $\omega_k = (gk)^{\frac{1}{2}}$ is the angular frequency of a linear gravity wave of wavenumber k. [Note that in Ref. (13) these equations were expressed in terms of the slope variables

$$q_{\underset{\sim}{k}}(t) \equiv k\, a_{\underset{\sim}{k}}(t) \exp(i\,\omega_k t) . \tag{4}$$

The coefficients C in Eqs. (3) are related to the coefficients Γ of Ref. (13) by the relations

$$C^{\underset{\sim}{k}\underset{\sim}{n}}_{\underset{\sim}{\ell}\underset{\sim}{p}} = (\ell pn/k)\,\Gamma^{\underset{\sim}{k}\underset{\sim}{n}}_{\underset{\sim}{\ell}\underset{\sim}{p}} ,$$

$$C^{\underset{\sim}{k}}_{\underset{\sim}{\ell}\underset{\sim}{p}} = (\ell p/k)\,\Gamma^{\underset{\sim}{k}}_{\underset{\sim}{\ell}\underset{\sim}{p}} ,$$

$$C^{\underset{\sim}{k}\underset{\sim}{p}}_{\underset{\sim}{\ell}} = (\ell p/k)\,\Gamma^{\underset{\sim}{k}\underset{\sim}{p}}_{\underset{\sim}{\ell}} . \ ]$$

We consider now a narrow packet of waves near a fixed wave number $\underset{\sim}{K} = K\,\hat{\imath}$, directed parallel to the x-axis. In this case we can write the complex surface amplitude Z in the form

$$Z(\underset{\sim}{x},t) = \exp[i(\underset{\sim}{K}\cdot\underset{\sim}{x} - \omega_K t)]\, G(\underset{\sim}{x},t),$$

$$G(\underset{\sim}{x},t) = {\sum_{\underset{\sim}{\ell}}}' a_{\underset{\sim}{K}+\underset{\sim}{\rho}} \exp[i(\underset{\sim}{\rho}\cdot\underset{\sim}{x} + \omega_K t)] , \tag{5}$$

where the primed summation implies that

$$\rho \ll K . \tag{6}$$

Equations (3) can be re-expressed in terms of G, using the second of Eqs. (5). The second order terms in (3) do not contribute

because of the constraints on wavenumbers implied by the δ-functions. The expression $\omega_{|\underset{\sim}{K}+\underset{\sim}{\rho}|}$ is expanded to second order in $\underset{\sim}{\rho}$ and we set

$$C^{\underset{\sim}{k}\underset{\sim}{n}}_{\underset{\sim}{\ell}\underset{\sim}{p}} \cong C^{\underset{\sim}{K}\underset{\sim}{K}}_{\underset{\sim}{K}\underset{\sim}{K}} = -K^2\omega_K/2 .$$

The resulting equation for G is then the nonlinear Schrödinger equation

$$i\left(\frac{\partial G}{\partial t} + c_g\frac{\partial G}{\partial x}\right) = \left[\omega_K/(8K^2)\right]\left[\frac{\partial^2 G}{\partial x^2} - 2\frac{\partial^2 G}{\partial y^2} + 4|G|^2 G\right] . \tag{7}$$

Here $c_g \equiv \frac{d\omega_K}{dK}$ is the group velocity of the wavetrain at wavenumber K. To describe waves in one-dimension only, we write $G = G(x,t)$ and drop the term involving y-derivatives from Eq. (7).

The one dimensional solution to Eq. (7) corresponding to an envelope soliton is of the form[3,5,7]

$$G(x,t) = A_0\,\mathrm{sech}\left[\sqrt{2}\; m\, K(x - x_0 - v_g\, t)\right]\exp\left[i(qx - \Omega t + \phi_0)\right] \tag{8}$$

where q, ϕ_0, x_0 and A_0 are real parameters and

$$m = K A_0$$

$$v_g = c_g + q\frac{d^2\omega_K}{dK^2} ,$$

$$\Omega = q\,c_g + \frac{1}{2}q^2\frac{d^2\omega_K}{dK^2} + m^2\omega_K/4 . \tag{9}$$

The "centered soliton," corresponding to $q = 0$, is of the form

$$G(x,t) = A_0\,\mathrm{sech}(\sqrt{2}\; m\, K\,\xi)\exp[\,(-i\omega_K m^2 t/4) + i\phi] . \tag{10}$$

where

$$\xi \equiv x - x_0 - c_g t \tag{11}$$

and ϕ is a constant.

For later reference, we quote the Benjamin-Feir[14] solution to Eq. (7), describing the interaction of two sinusoidal wavetrains. This is of the form

$$G = (A_0 + \epsilon A_1) \exp[i(\theta_0 + \epsilon \theta_1)] . \tag{12}$$

Here A_0 is a constant, ϵ is a very small parameter, and

$$\theta_0 = - \omega_K m^2 t/2 . \tag{13}$$

We write

$$A_1 = \mathrm{Re}[\exp(i q \xi + \gamma t)] \tag{14}$$

to find that

$$\frac{\partial^2 \theta_1}{\partial \xi^2} = - \left[2 \Big/ \frac{d^2 \omega_K}{dK^2} \right] \left[\frac{\partial A_1}{\partial t} \right] \Big/ A_0 \tag{15}$$

and

$$\gamma = \pm (\omega_K q/8K^2)[8A_0^2 K^4 - q^2]^{\frac{1}{2}} \tag{16}$$

The maximum growth rate, using Eq. (16), occurs for

$$q = \pm 2 K^2 A_0 . \tag{17}$$

For this value of q,

$$\gamma = \pm \sqrt{2}\ \omega_K (K A_0)^2 . \tag{18}$$

On writing $m \equiv K A_0$ for the slope of the large amplitude wave, we see that

$$\tau_{BF} \equiv (\sqrt{2}\ \omega_K m^2)^{-1} \tag{19}$$

describes an e-folding time for the Benjamin-Feir interaction. Reference to the nonlinear term in Eq. (7) suggests that τ_{BF} can be taken as a characteristic time scale for nonlinear interactions to develop, providing that the wavenumber separation between discrete Fourier modes in Eq. (2) is less than [see Eq. (17)]

$$\Delta k = 2\sqrt{2}\ K m. \tag{20}$$

For the soliton depicted by Eq. (8) the characteristic time for dispersive spreading is also τ_{BF}. The balancing of this spreading by the nonlinear "peaking" effect leads to the steady solution (8).

If waves in only a single dimension are considered, we can re-write Eq. (7) in the simpler form

$$i \frac{\partial G}{\partial t} = [\omega_K/(8K^2)] \left[\frac{\partial^2 G}{\partial \xi^2} + 4 |G|^2 G \right] . \tag{21}$$

It has been shown by Zakharov and Shabat[8] that solutions to Eq. (21) may be constructed as a superposition of several solitons and a non-soliton component. The solitons remain as stable entities in spite of the presence of the nonlinear coupling term in Eq. (21). This stability of the soliton solutions of Eq. (21) does not imply a corresponding stability of the soliton solutions to the modal rate equations (3), since the derivation of Eq. (21) from Eqs. (3) required the condition (5), i.e., that the surface wave spectrum is narrow.

III. COMPARISON WITH THE FEIR EXPERIMENTS

The numerical code described in Ref. (13) integrates Eqs. (3) for a specified set of modes, but is restricted to one-dimension, with all wavenumbers parallel to, say, the x-axis. A "fetch" L is specified with periodic boundary conditions at $x = -\frac{L}{2}$ and $x = \frac{L}{2}$. The mode spacing is $\Delta k = 2\pi/L$.

To integrate Eqs. (3) the initial amplitudes $a_n(0)$ $(k_n = n\Delta k,\ n = 1, 2, \cdots)$ at $t = 0$ are specified.

If the initial state of Eq. (3) is prepared to be that of a soliton, then the nonlinear interactions should not change the surface structure, i.e., the soliton should persist as it propagates along the water surface. The initial conditions for Eq. (3) are obtained by taking the Fourier transform of the envelope function at time $t = 0$, to obtain the mode amplitudes

$$a_n(0) = \frac{1}{L}\int_{-\infty}^{\infty} G(\xi,0)\exp[i(K - k_n)\,\xi]d\xi\,, \qquad (22)$$

where $G(\xi,0)$ is given in Eq. (10). Integrating and normalizing Eq. (22), we obtain for the mode amplitudes of an initial soliton

$$a_n(0) = a_N(0)\,\mathrm{sech}\left[\frac{(N - n)\pi\,\Delta k}{\sqrt{8}\ m\,K}\right] \qquad (23)$$

with the central mode given by wavenumber $K = N\Delta k$.

In calculations, Eq. (23) is used to represent the initial soliton by a finite number of modes. In Figure 1a is shown an envelope function constructed from fifteen modes with the parameters, $K = 0.2516\ \mathrm{cm}^{-1}$, $\Delta k = 0.01\ \mathrm{cm}^{-1}$ and $m = 0.064$, where m is the slope of the soliton. This envelope is given by the absolute value of

$$G(x,t) = \sum_n \frac{q_n(t)}{k_n}\exp[i(N - n)\Delta k(x - c_g t)] \qquad (24)$$

where

$$c_g \equiv (\omega_n - \omega_N)/\Delta k(N - n)$$

is the group velocity of the central mode and the slope variables from Eq. (4) have been used. The modal rate equations in Ref. (13) are written in terms of the mode slopes, i.e., the q's, so that in Fig. 1 and in all subsequent figures involving the envelope, it is the absolute value of Eq. (24) that is plotted. The mode slopes for Fig. 1 are listed in Table I.

In Fig. 1b the displacement of the water surface is depicted for the above soliton. The surface displacement is described by Eqs. (1) and (4). The parameters for this example were selected to correspond to the wavepulse experiments conducted by Feir.[9] The initial amplitude of the central mode in Eq. (23) is obtained from the experiment using the expression

$$a_N(0) = G(x=0)\left\{\sum_n \mathrm{sech}[\pi\Delta k(n - N)/\sqrt{8}\ mK]\right\}^{-1} \qquad (25)$$

where $m = 0.064$ and $G(x = 0) = 0.254$ cm for the first trace in Fig. 3 of Ref. (9) yielding $a_N(0) = 0.056$ cm. The slope of the soliton is given by the sum of the mode slopes, i.e.,

$$m = K\sum_n \frac{q_n(0)}{k_n} \qquad (26)$$

which is also equal to the central wavenumber times the maximum surface displacement.

Figure 1 analytically models the shape of the pulse generated in Feir's experiment as measured four feet from the wavemaker. At a distance of twenty-four feet from this point, i.e., twenty-eight feet down the tank, the pulse amplitude is one half its initial value. This damping of the pulse is simulated in the present calculation using a phenomenological viscosity coefficient in the rate equations. The linear amplitude damping coefficient yields

$$G(x,t) = G(x,0)\exp(-\alpha t) \qquad (27)$$

where t is given by the ratio of the distance traveled to the group velocity. The decay rate is given by $\alpha = 0.03\ \text{sec}^{-1}$, or in terms of the viscosity coefficient $\nu \equiv \alpha/K^2 = 0.47\ \text{cm}^2/\text{sec}$.

Feir's discussion[9] does not include the concept of a soliton. The analysis of Chu and Mei,[3] however, compares the evolution of the pulse modeled as a soliton with the experimental results. As they pointed out the dominant effect is the attenuation in amplitude due to the short time of evolution; i.e., short compared with the e-folding time which is given in Table I as 11 sec. In Fig. 2 the results of the present calculation are given for the pulse after 24 seconds or approximately 24 feet from the initial point. The shape of the pulse is virtually unchanged from Fig. 1. The normalization has changed from 0.254 cm, however, to 0.115 cm; a 0.45 reduction in amplitude.

Reference (9) describes the launching of six pulse shapes, all with the same central mode number and length of modulation, but with increasing amplitudes. The simulation of run (1), shown in Figs. 1 and 2, indicates that this pulse is very close to a soliton in shape. The remaining runs, with their increased amplitudes, must therefore not be

solitons. The modulational instability of these waveforms causes these pulses to breakup into one or more stable solitons.[16] This interpretation is consistent with what is observed in the latter runs of Ref. (9).

In Fig. 3 the last of the six runs from Ref. (9) is simulated. Since only the amplitude was increased between this and the first run, the mode slopes of the soliton are simply scaled by a factor of four to correspond with the experiment. The viscosity coefficient has been modified in this case to again give the gross attenuation of the pulse. These quantities, along with the slope of the pulse are listed in the second column of Table I.

The initial pulse is depicted in Fig. 3a, as it would be at the wave generator rather than at four feet along the tank as was the soliton in Figs. 1 and 2. This is admittedly not a complete simulation of the experiment. After traveling 28 feet down the tank, however, Fig. 3b shows the same general structure observed in Ref. (9) for the breakup of the initial waveform.

IV. STABILITY

We discuss first the stability of the soliton solution to Eq. (7) given by Eq. (10) when a small sinusoidal ripple is impressed on it transverse to the direction of soliton propagation.

Equation (7) may be rewritten in a coordinate system translating with a velocity c_g parallel to the x-axis, i.e., $\xi = x - c_g t$, in the more convenient form

$$i \frac{\partial G}{\partial t} = \frac{\omega_K}{8K^2} \left[\frac{\partial^2 G}{\partial \xi^2} - 2 \frac{\partial^2 G}{\partial y^2} + 4K^2 |G|^2 G \right] . \tag{28}$$

From Eq. (28) we obtain the relation for the wave energy (in scaled units)

$$i \frac{\partial}{\partial t} |G|^2 = \frac{\omega_K}{8K^2} \left[\frac{\partial}{\partial \xi} \left(G^* \frac{\partial G}{\partial \xi} - G \frac{\partial G^*}{\partial \xi} \right) - 2 \frac{\partial}{\partial y} \left(G^* \frac{\partial G}{\partial y} - G \frac{\partial G^*}{\partial y} \right) \right] . \tag{29}$$

A solution having finite extent in the ξ-direction and periodic boundary conditions in the y-direction then satisfies the energy integral

$$\int_\Sigma |G|^2 \, d\xi \, dy = \text{constant} \tag{30}$$

over the surface area Σ. A developing instability thus extracts energy from the soliton.

The solution of the nonlinear Schrödinger equation which we investigate is of the form

$$G = G_s + Y(\xi,t) \cos(\ell y) \exp(-i\omega_K m^2 t/4) \tag{31}$$

where G_s represents the soliton solution (10) and Y is assumed to

be very small relative to the amplitude of the soliton. This is our transverse perturbation. It is convenient to introduce the dimensionless variables

$$\tau \equiv \omega_K t/8$$

$$s \equiv \sqrt{2} \, m K \xi \tag{32}$$

and to write the perturbation amplitude as the complex function

$$Y(s,t) = U(s,\tau) + i V(s,\tau) , \tag{33}$$

where U and V are real. Substituting expression (31) into the equation of evolution (28), linearizing in Y, and equating to zero the real and imaginary parts of the resulting expression, yields the coupled equations

$$-\frac{\partial V}{\partial \tau} = \frac{\partial^2 U}{\partial s^2} + (H + W)U$$

and

$$\frac{\partial U}{\partial \tau} = \frac{\partial^2 V}{\partial s^2} + (H - W)U . \tag{34}$$

The coefficient functions in Eq. (34) are given by

$$H = Q - 1 + 4 \operatorname{sech}^2(s) ,$$

$$W = 2 \operatorname{sech}^2(s) \tag{35}$$

and

$$Q = \ell^2/(mK)^2 . \tag{36}$$

Consider first the case of a simple exponentially growing instability, for which we write

$$U = u(s) \exp(E\tau)$$

$$V = v(s) \exp(E\tau).$$

When substituted into Eq. (34) this yields

$$-Ev = u_{ss} + (H + W)u$$

$$Eu = v_{ss} + (H - W)v , \tag{37}$$

where the subscript notation for derivatives has been adopted, i.e., $u_s \equiv du/ds$, etc. For stable oscillating perturbations we would, on the other hand, write

$$U = u(s) \sin(E\tau)$$

$$V = v(s) \cos(E\tau)$$

which when substituted in Eq. (34) yields

$$Ev = u_{ss} + (H + W)u$$

$$Eu = v_{ss} + (H - W)v . \tag{38}$$

Since neither set of Eqs. (37) and (38) is self-adjoint, we have no a priori assurance that normalizable solutions will be found with E real.

At this point it might be observed that our discussion is similar to that of Schmidt,[17] who studied the stability of a plasma wave soliton. His soliton was of the form (10), but his equation describing the transverse perturbation was somewhat different from Eqs. (34). Schmidt[17] observed that for the case

$$Q = E = 0 ,$$

Eqs. (37) and (38) have two sets of solutions:

Even Parity: $v = v^{(0)} = \operatorname{sech} s$

$u = 0$

Odd Parity: $v = 0$

$$u = u^{(0)} = dv^{(0)}/ds , \tag{39}$$

where the superscript indicates the condition $Q = E = 0$.

The solutions [Eqs. (39)] suggest using perturbation theory to analyze Eqs. (37) and (38) for small Q, or long wavelength perturbations. Consider first the odd parity case and define the operators

$$\underset{\sim}{L} \equiv (d^2/ds^2) + 2 \operatorname{sech}^2 s - 1$$

$$\underset{\sim}{L}' \equiv (d^2/ds^2) + 6 \operatorname{sech}^2 s - 1 . \tag{40}$$

Equations (37) can then be rewritten

$$\underset{\sim}{L}'u = - Ev - Qu$$

$$\underset{\sim}{L}'v = Eu - Qv + 4 v \operatorname{sech}^2 s \tag{41}$$

and, using Eq. (39),

$$\underset{\sim}{L}' u^{(0)} = 0 . \tag{42}$$

Multiplying both expressions in Eqs. (41) by $u^{(0)}$ and integrating over all s , using Eqs. (42) and substituting the first expression into the second, yields

$$E^2 = -Q^2 + 4Q \int_{-\infty}^{\infty} u^{(0)} v \operatorname{sech}^2 s \, ds \Big/ \int_{-\infty}^{\infty} u^{(0)} v \, ds . \tag{43}$$

If we write the solution to Eq. (41) as a first order correction term,

$$v = E v^{(1)} , \tag{44}$$

then from the second expression in Eq. (41), to lowest order in E and Q, we obtain [see Eqs. (40)]

$$\underset{\sim}{L} v^{(1)} = u^{(0)} . \tag{45}$$

To evaluate the ratio of integrals in Eq. (43) and thereby obtain the eigenvalue E, we use the relations

$$\int_{-\infty}^{\infty} u^{(0)} v^{(1)} \operatorname{sech}^2 s \, ds = -\frac{1}{6} = -\frac{1}{4} \int_{-\infty}^{\infty} [u^{(0)}]^2 ds$$

$$\int_{-\infty}^{\infty} u^{(0)} v^{(1)} ds = -\frac{1}{2} = -\frac{1}{4} \int_{-\infty}^{\infty} [v^{(0)}]^2 ds .$$

The first of these relations derives directly from Eq. (41), whereas the second is the result of a numerical integration. Neglecting Q^2 in Eq. (43) we obtain the eigenvalue

$$E \approx 1.16 \, Q^{\frac{1}{2}} . \tag{46}$$

Equation (45) was numerically evaluated for later use. Also the above integrals were evaluated numerically as a test of the solution.

An analysis similar to the above, starting with the even parity zeroth order solution [see Eqs. (39)] gave stable, oscillating modes [the case described by Eqs. (38)] for small Q. This contrasts with the results of Schmidt[17] for plasma waves, where the even parity solution was unstable.

For a shorter wavelength perturbation, corresponding to $Q \gg 1$, Eqs. (34) have the approximate form

$$-\partial V/\partial \tau = U_{ss} + (Q - 1)U$$

$$\partial U/\partial \tau = V_{ss} + (Q - 1)V . \tag{47}$$

These equations describe the propagation of linear waves, decoupled from the soliton. An impressed ripple of short wavelength [consistent with the assumption (5)] will thus tend to propagate in accordance with the linear dispersive wave equation.

For $Q > 1$ there is no normalizable solution to Eqs. (37) and (38) when $E = 0$,[18] so a transition from simple exponential growth to simple oscillatory behavior is not possible in the range $1 < Q < \infty$.

Equations (34) were numerically integrated using the perturbation solution $u = u^{(0)}$, $v = Ev^{(1)}$ as the starting condition for $\tau = 0$.[19] For $Q \leq 1$ simple exponential growth consistent with the result (46) seemed to occur (for the two exponentiating periods that the calculation was continued). For $Q = 2$ the U and V solutions oscillated. Growth was not observed within the accuracy of the

calculation, but propagation away from the soliton did occur. For $Q = 1.5$ propagation away from the soliton was observed, but at a slower rate. Some growth seemed to occur. The oscillatory motion for the larger Q value is consistent with our conclusions based on Eqs. (47).

Defining the e-folding rate γ by the relation $\gamma t = E\tau$, we have summarized in Fig. 4 the instability discussed above. The quantity $\gamma\tau_{BF}$ [Eq. (19)] is plotted against $Q^{\frac{1}{2}} = \ell/(mK)$. Due to the limited accuracy of our calculations, the growth rate in the interval $Q > 1$ is not shown.

We now discuss the propagation of two specific solitons through a train of waves of wave number significantly different from that of the soliton. For both solitons the interval L was chosen as 100 m, so the wave-number interval was $\Delta k = 0.0628\ m^{-1}$. The starting Fourier amplitudes were obtained using Eq. (22). The initial slopes $q_n(0)$ are given in columns (3) and (4) of Table I.

The soliton of column (3) has a central mode number $N = 10$, with amplitudes in the range $6 \leq n \leq 14$. We shall refer to this as the "fat" soliton, since its broad spectrum would seem to violate the conditions under which the nonlinear Schrödinger equation was derived.

Equations (3) were integrated for an interval of 20 seconds for the fat soliton with the initial conditions of column (3) in Table I. The wave height ζ, as obtained from Eq. (3), is shown in Figs. 5a,b at $t = 0$ and 50 secs for the fat soliton and in Figs. 6a,b for the "thin" soliton. The corresponding envelope function G for the thin soliton is shown in Figs. 7a,b for $t = 0$ and 50 secs. Again no distortion is discernable.

We now study the interaction of these two solitons with other wavetrains. For the first case we let the thin soliton interact with shorter wavelength waves, corresponding to the mode numbers $n = 32$ and 33. The starting slopes at $t = 0$ were $q_{32}(0) = 0.1$ and $q_{33}(0) = 0.15$, with respective phases of 0° and 45°. The wave amplitude ζ is shown in Figs. 8a,b,c at $t = 0$, 30, and 50 seconds, respectively. The envelope function G is shown at these times in Figs. 9a,b,c. Little distortion has occurred at 30 secs. At 50 seconds, however, the soliton edges show an appreciable distortion. It is here where G is small that a modest phase distortion can most readily upset the cancellation of Fourier amplitudes. These results certainly suggest that eventually the soliton would be destroyed by interaction with a spectrum of short wavelength waves.

The next example studied of soliton interaction involved a train of long wavelength waves, with mode numbers $n = 6$ and 7. The starting slopes were $q_6(0) = 0.1$ and $q_7(0) = 0.15$, and the thin soliton was again used. The displacement ζ is shown in Figs. 10a-f at various times in the interval $0 \leq t \leq 20$ seconds. Marked distortion occurs at 2 secs, about one wave period at the soliton carrier frequency. The soliton substantially recovers its shape at 10 seconds and then again at 20 seconds. It would appear that the soliton is being compressed and stretched by the orbital fluid velocity of the interacting wavetrain and that this is to some extent reversible. To investigate this further, the above calculation was repeated but at 10 seconds the amplitudes q_6 and q_7 were set equal to zero. At this time the soliton has the form shown in Fig. 10d. At 20 and 50 seconds it has amplitude shown in Figs. 11a,b. The corresponding envelope function is shown in Figs. 12a,b at 20 and 50 seconds. It is not clear in this time interval that the soliton is undergoing a progressive distortion. The leading edge (to the right) of the

envelope function does seem to be steepening somewhat at 50 seconds. A similar asymmetric distortion was noted by Lighthill.[1]

The final illustration studied of soliton interaction was that of the fat soliton interacting with a train of longer waves. These corresponded to modes $n = 3$ and $n = 4$, with starting slopes $q_3(0) = 0.06$ and $q_4(0) = 0.09$ and respective phases of 0° and 45°. The soliton is shown in Figs. 13a-d at times from 0 to 20 seconds. The soliton in this case does not seem to recover, but progressively looses its initial waveform. It should be recalled that this was thought to be a "marginal" soliton.

The above examples suggest that a random field of waves of wavelength much shorter than that of the soliton will probably break up the soliton, but rather slowly. A random wave field of much longer waves can probably destroy a soliton in a few wave periods. A periodic train of long waves distorts the soliton, but it shows some recovery.

V. SOLITONS IN AN AMBIENT WAVE FIELD

The preceding sections were concerned with the persistence of waveforms (usually solitons) both when isolated and when interacting with simple wavetrains of much different frequency. When discussing wave fields, such as present on the surface of the ocean, one often makes use of the notion of a wavepacket or pulse to describe the behavior of some component of the wave field. In this section we consider some statistical aspects of solitons when immersed in an ambient spectrum of waves.

Consider the complex surface displacement [Eq. (2)] to have mode amplitudes of the form

$$a_{\underset{\sim}{k}} = A(\underset{\sim}{k}) + \sum_{\lambda=1}^{N} C_\lambda(\underset{\sim}{k}) \tag{48}$$

where the $A(\underset{\sim}{k})$'s are the amplitudes of the ambient wave field and the $C_\lambda(\underset{\sim}{k})$'s describe the solitons of which there are N. The homogeneous spectrum of the surface wave field over an area of ocean Σ is given by

$$\Psi(\underset{\sim}{k}) = \frac{\Sigma}{(2\pi)^2} \frac{1}{2} \langle \, | a_{\underset{\sim}{k}} |^2 \, \rangle \tag{49}$$

where the brackets denote an average over many realizations of the surface wave field and the $a_{\underset{\sim}{k}}$'s are given by Eq. (48).

Assuming the $A(\underset{\sim}{k})$'s to be independent random variables with a Gaussian distribution and also independent of the $C_\lambda(\underset{\sim}{k})$'s, Eq. (49) can be rewritten as

$$\Psi(\underset{\sim}{k}) = [\Sigma/2(2\pi)^2]\ [\Phi(\underset{\sim}{k}) + h(\underset{\sim}{k})] \qquad (50)$$

where

$$\Phi(\underset{\sim}{k}) \equiv \langle\ |\ A(\underset{\sim}{k})\ |^2\ \rangle$$

$$h(\underset{\sim}{k}) \equiv \langle \sum_{\lambda} |\ C_\lambda(\underset{\sim}{k})\ |^2\ \rangle\ . \qquad (51)$$

It is not clear how to perform the formal average over the soliton distribution in Eq. (51), but it should involve averaging over the set of parameters $\xi = (m, \underset{\sim}{x}_0, \underset{\sim}{K}, \Phi)$ defined in Section II.

In the absence of solitons the surface wave-field amplitudes have been assumed to be strictly uncorrelated so that the fourth order cumulant (Γ_4) of the distribution vanishes. In general, it is of the form

$$\Gamma_4(\underset{\sim}{k}_1, \underset{\sim}{k}_2, \underset{\sim}{k}_3, \underset{\sim}{k}_4) \equiv \langle\ a_{\underset{\sim}{k}_1}\ a^*_{\underset{\sim}{k}_2}\ a_{\underset{\sim}{k}_3}\ a^*_{\underset{\sim}{k}_4}\ \rangle - \langle a_{\underset{\sim}{k}_1}\ a^*_{\underset{\sim}{k}_2}\rangle\langle a_{\underset{\sim}{k}_3}\ a^*_{\underset{\sim}{k}_4}\ \rangle$$

$$- \langle a_{\underset{\sim}{k}_1}\ a^*_{\underset{\sim}{k}_4}\rangle\langle a_{\underset{\sim}{k}_3}\ a^*_{\underset{\sim}{k}_2}\ \rangle\ . \qquad (52)$$

After some algebraic manipulation and use of Eqs. (48) - (51), Eq. (52) reduces to

$$\Gamma_4(\underset{\sim}{k}_1, \underset{\sim}{k}_2, \underset{\sim}{k}_3, \underset{\sim}{k}_4) = \left\langle \sum_{\lambda=1}^{N} C_\lambda(\underset{\sim}{k}_1)C_\lambda^*(\underset{\sim}{k}_2)C_\lambda(\underset{\sim}{k}_3)C_\lambda^*(\underset{\sim}{k}_4) \right\rangle$$

$$+ h(\underset{\sim}{k}_1)h(\underset{\sim}{k}_3)\left[\delta_{\underset{\sim}{k}_1-\underset{\sim}{k}_2}\,\delta_{\underset{\sim}{k}_3-\underset{\sim}{k}_4} + \delta_{\underset{\sim}{k}_1-\underset{\sim}{k}_4}\,\delta_{\underset{\sim}{k}_2-\underset{\sim}{k}_3}\right]$$

$$\times \left[\langle N(N-1)\rangle/\langle N^2\rangle - 1\right]\ . \qquad (53)$$

For $\langle N \rangle \gg 1$, i.e., when many solitons are present in the area Σ, the second term in Eq. (53) can be neglected.

Assuming each of the solitons to have the structure given by Eq. (10); Eq. (53) can be rewritten as

$$\Gamma_4(\underset{\sim}{k}_1, \underset{\sim}{k}_2, \underset{\sim}{k}_3, \underset{\sim}{k}_4) \approx \langle N \rangle (2\pi^2/\Sigma)^2 \left\langle K^{-8} \prod_{i=1}^{4} \delta(k_{i\perp}) \operatorname{sech}\left[\frac{(k_{i\parallel} - K)\pi}{\sqrt{8}\ mK}\right] \right\rangle$$

$$\times\ \delta_{\underset{\sim}{k}_1+\underset{\sim}{k}_2-\underset{\sim}{k}_3-\underset{\sim}{k}_4} \qquad (54)$$

where $k_{i\perp}$ and $k_{i\parallel}$ are the components of $\underset{\sim}{k}_i$ perpendicular and parallel to $\underset{\sim}{K}$, respectively.

As mentioned above, we lack sufficient information to rigorously evaluate the indicated statistical average in Eq. (53). We thus try a simple model, for mathematical convenience, replacing the δ-functions by narrow Gaussian functions, setting $\operatorname{sech} x \sim \exp(-x^2/2)$, and averaging the soliton parameters over uniform intervals. If we choose all the wavenumbers to be parallel (appropriate for example to observations by monostatic, multi-frequency radar[20]) and set

$$k_1 = k_0 + \eta_1, \qquad k_2 = k_0 - \eta_2, \qquad k_3 = k_0 - \eta_1, \qquad k_4 = k_0 + \eta_2,$$

our model gives

$$\Gamma_4(k_1, k_2, k_3, k_4) \sim A \exp\left\{-(\pi/m)^2(\eta_1^2 + \eta_2^2)/8\ k_0^2\right\}\ . \qquad (51)$$

Here A is an unevaluated amplitude and m a "characteristic" slope parameter. The cumulant is thus positive definite and decreases with increasing spectral width of the soliton.

TABLE I: Slope amplitudes [see Eq. (42)] for the "solitons" studied.

Mode Number n - N	Mode Slope Amplitudes of Solitons -- $q_n(0)$			
-7	10^{-5}	4×10^{-5}	---	---
-6	2.33×10^{-4}	9.32×10^{-4}	---	---
-5	5.36×10^{-4}	2.14×10^{-3}	---	---
-4	1.21×10^{-3}	4.84×10^{-3}	2.63×10^{-3}	2.68×10^{-3}
-3	2.66×10^{-3}	1.06×10^{-2}	6.07×10^{-3}	5.35×10^{-3}
-2	5.6×10^{-2}	2.24×10^{-2}	1.33×10^{-2}	1.02×10^{-2}
-1	1.03×10^{-2}	4.12×10^{-2}	2.54×10^{-2}	1.72×10^{-2}
0	1.41×10^{-2}	5.64×10^{-2}	3.54×10^{-2}	2.21×10^{-2}
1	1.22×10^{-2}	4.88×10^{-2}	3.11×10^{-2}	1.95×10^{-2}
2	7.73×10^{-3}	3.09×10^{-2}	1.99×10^{-2}	1.31×10^{-2}
3	4.34×10^{-3}	1.74×10^{-2}	1.13×10^{-2}	7.82×10^{-3}
4	2.34×10^{-3}	9.36×10^{-2}	6.14×10^{-3}	4.47×10^{-3}
5	1.25×10^{-3}	5.0×10^{-3}	---	---
6	6.64×10^{-4}	2.66×10^{-3}	---	---
7	3.5×10^{-4}	1.4×10^{-3}	---	---
Viscosity coefficient-ν	0.47 cm^2/sec	0.19 cm^2/sec	0.0	0.0
Soliton Slope-m	0.064	0.256	0.16	0.11
Central Wavenumber-K	0.2516 cm^{-1}	0.2516 cm^{-1}	0.628 m^{-1}	1.0 m^{-1}
Mode Spacing-Δ k	0.01 cm^{-1}	0.01 cm^{-1}	0.0628 m^{-1}	0.0628 m^{-1}
Nonlinear Growth time-τ_{BF}	11.0 sec.	0.69 sec.	11.1 sec.	18.5 sec.

FOOTNOTES AND REFERENCES

* This work was supported in part by the Energy Research and Development Agency.

1. M. J. Lighthill, J. Inst. Math. Applics 1, 296 (1965); Proc. Roy. Soc. A299, 28 (1967).
2. D. J. Benney and A. C. Newell, J. Math. Phys. 46, 133 (1967).
3. V. H. Chu, and C. C. Mei, J. Fluid Mech. 41, 873 (1970); ibid. 47, 337 (1971),
4. A. Davey, J. Fluid Mech. 53, 769 (1972).
5. B. M. Lake and H. C. Yuen, to be published.
6. G. B. Whitham, J. Fluid Mech. 22, 273 (1965); ibid. 27, 399 (1967); Proc. Roy. Soc. A299, 6 (1967).
7. For a review of the theory of solitons, see A. C. Scott. F. Y. F. Chu and D. W. McLaughlin, Proc. of IEEE 61, 1443 (1973).
8. V. E. Zakharov and A. B. Shabat, Sov. Phys. JETP 34, 62 (1972).
9. J. E. Feir, Proc. Roy. Soc. A283, 54 (1965).
10. O. M. Phillips. J. Fluid Mech. 9, 193 (1960).
11. M. S. Longuet-Higgins, J. Fluid Mech. 12, 321 (1962).
12. K. Hasselmann, J. Fluid Mech. 12, 481 (1962).
13. B. J. West, K. M. Watson, and J. A. Thomson, Phys. Fluids 17, 1059 (1974).
14. T. B. Benjamin and J. E. Feir, J. Fluid Mech. 27, 417 (1967).
15. K. M. Watson and B. J. West, in process of publication in J. Fluid Mech., have given a more useful modal analysis based on Eq. (1), but with ϕ_s defined on the actual, displaced surface rather than the undisturbed surface. For our present application to narrow-band wave systems this distinction is not important.

16. H. Hasimoto and H. Ono, J. Phys. Soc. of Japan 33, 805 (1972).
17. G. Schmidt, Phys. Rev. Letters 34, 724 (1975).
18. In this case, Eqs. (37) and (38) are each equivalent to a one-dimensional Schrödinger equation with an attractive potential. If $Q > 1$, this would correspond to a bound state of positive energy.
19. We are indebted to Ralph Janda for doing this calculation.
20. We would like to thank Drs. A. M. Peterson, W. Munk, and R. Stewart for a discussion concerning their multi-frequency radar observations of surface wave scattering.

FIGURE CAPTIONS

Fig. 1. The soliton specified by the slope amplitudes of column (1), Table I, is shown at $t = 0$. (a) The envelope G and (b) the wave displacement ζ are normalized to 0.251 cm.

Fig. 2. The soliton of Fig. 1 and its envelope are shown at $t = 24$ seconds. (a) G and (b) ζ are normalized to 0.115 cm.

Fig. 3. Wave packet with slope amplitudes given in column (2) of Table I is shown in (a) for time $t = 0$. It is shown at $t = 24$ seconds in (b).

Fig. 4. The e-folding rate γ for soliton transverse instability is shown in units of the Benjamin-Feir time scale τ_{BF} [Eq. (19)]. The quantity Q is defined by Eq. (36).

Fig. 5. The "fat" soliton of column (3), Table I, is shown at (a) 0 seconds and (b) 20 seconds. The surface displacement is normalized to 24.7 cm and 23.48 cm, respectively.

Fig. 6. The "thin" soliton of column (4), Table I, is shown at (a) 0 seconds and (b) 50 seconds. The surface displacement is normalized to 10.19 cm and 9.91 cm, respectively.

Fig. 7. The envelope function for the soliton of Fig. 6 is shown at (a) 0 seconds with an A_0 of 10.19 cm and (b) 50 seconds with an A_0 of 9.91 cm.

Fig. 8. The thin soliton passing through an infinite wavetrain of higher frequency waves is depicted at time t with normalization A_0; (a) $t = 0$, $A_0 = 10.19$ cm; (b) $t = 30$, $A_0 = 9.9$ cm; (c) 50 seconds, $A_0 = 8.4$ cm.

Fig. 9. The envelope function for the interacting soliton of Fig. 8 is shown at time t and normalization A_0; (a) $t = 0$, $A_0 = 10.19$ cm; (b) $t = 30$, $A_0 = 9.0$ cm; (c) 50 seconds, $A_0 = 8.4$ cm.

Fig. 10. The thin soliton passing through a wavetrain of lower frequency waves is shown at time t and normalization A_0; (a) $t = 0$, $A_0 = 10.19$ cm; (b) $t = 2$, $A_0 = 21.27$ cm (c) $t = 8$, $A_0 = 20.32$ cm; (d) $t = 10$, $A_0 = 16.19$ cm; (e) $t = 18$, $A_0 = 17.11$ cm; (f) $t = 20$ seconds, $A_0 = 18.22$ cm.

Fig. 11. The soliton of Fig. 10 is shown for the case that the interacting wavetrain was damped to zero amplitude at 10 seconds. The times and maximum surface displacements are (a) 20 seconds, 16.42 cm and (b) 50 seconds, 16.11 cm.

Fig. 12. The envelope function, corresponding to the calculation shown in Fig. 11, is shown at time t with corresponding A_0's; (a) 20 seconds, 16.42 cm and (b) 50 seconds, 16.11 cm.

Fig. 13. The fat soliton passing through a lower frequency wavetrain is shown at times t with corresponding A_0's; (a) 0 seconds, 24.07 cm; (b) 2 seconds, 47.49 cm; (c) 10 seconds, 49.81 cm; (d) 20 seconds and 42.61 cm.

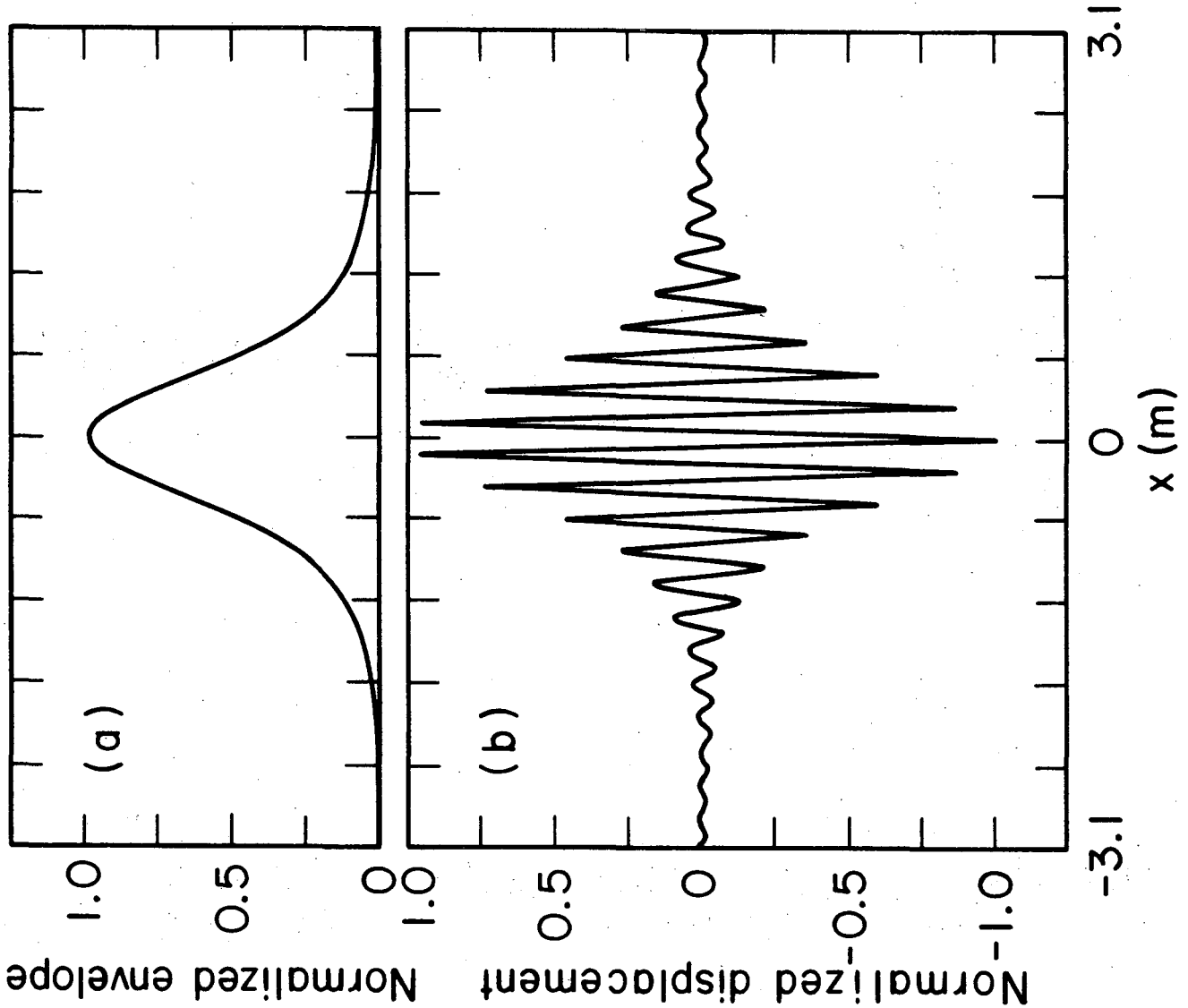

XBL756-3277

Fig. 1

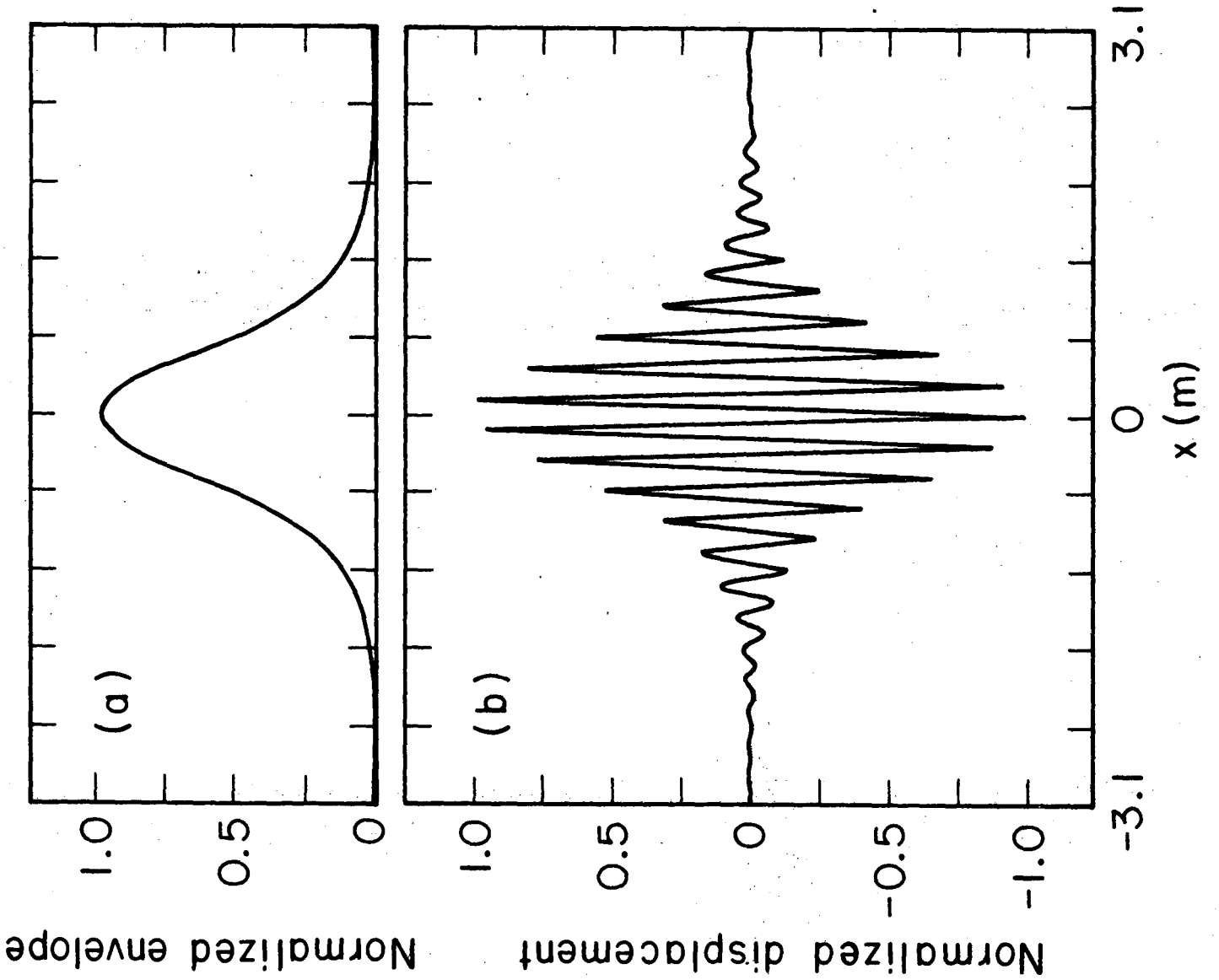

XBL756-3286

Fig. 2

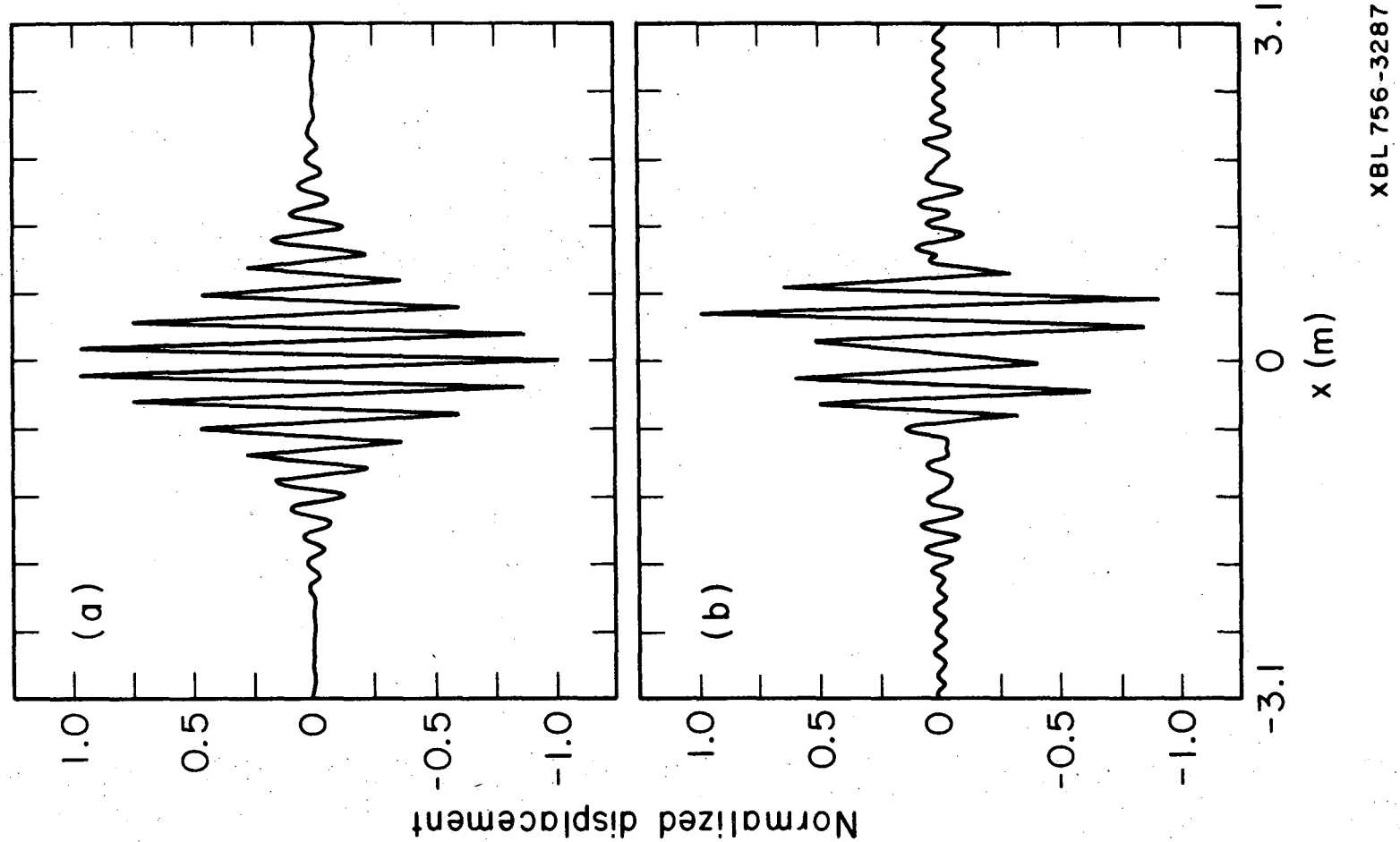

Fig. 3

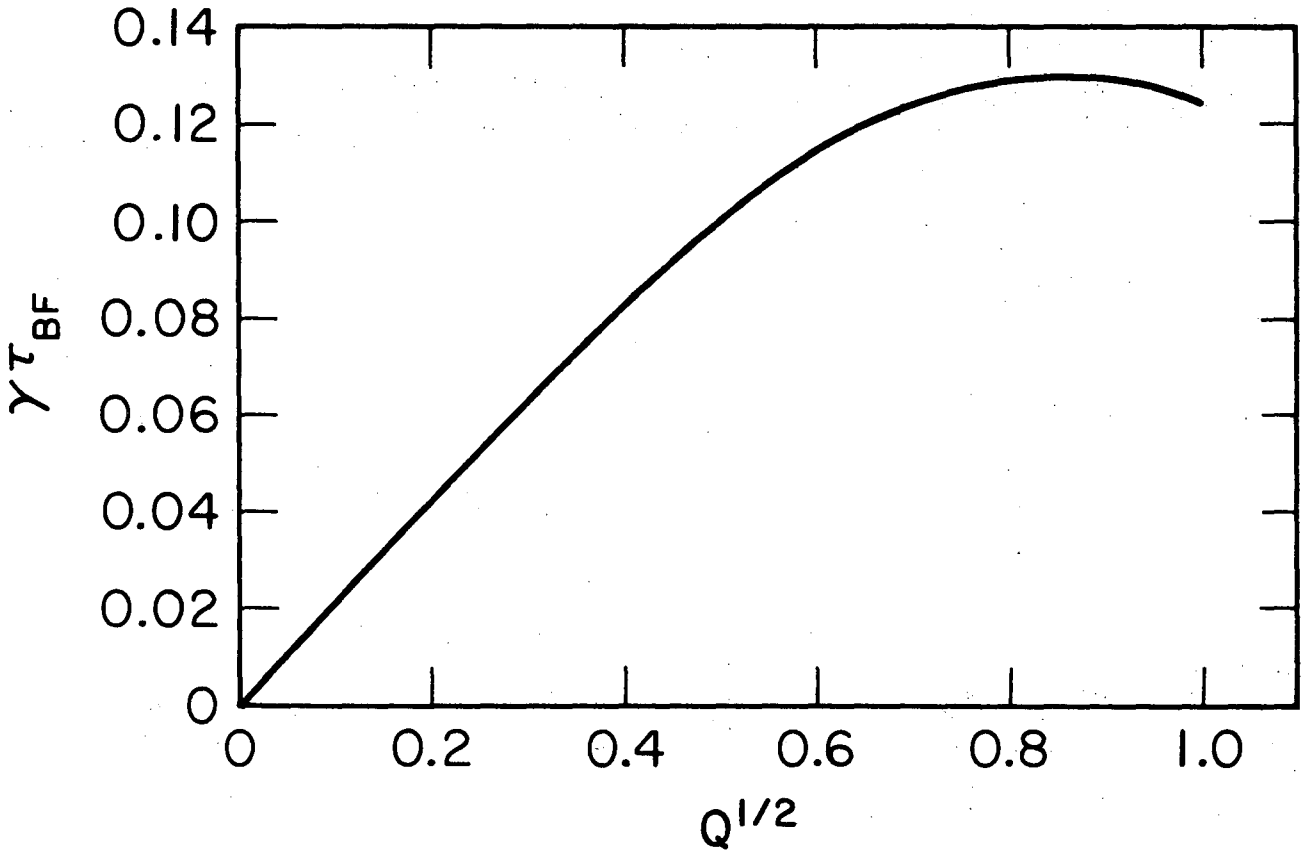
0.14
0.12
0.10
0.08
0.06
0.04
0.02
0
$\gamma\tau_{BF}$
0
0.2
0.4
0.6
0.8
1.0
$Q^{1/2}$
XBL 756-3278

Fig. 4

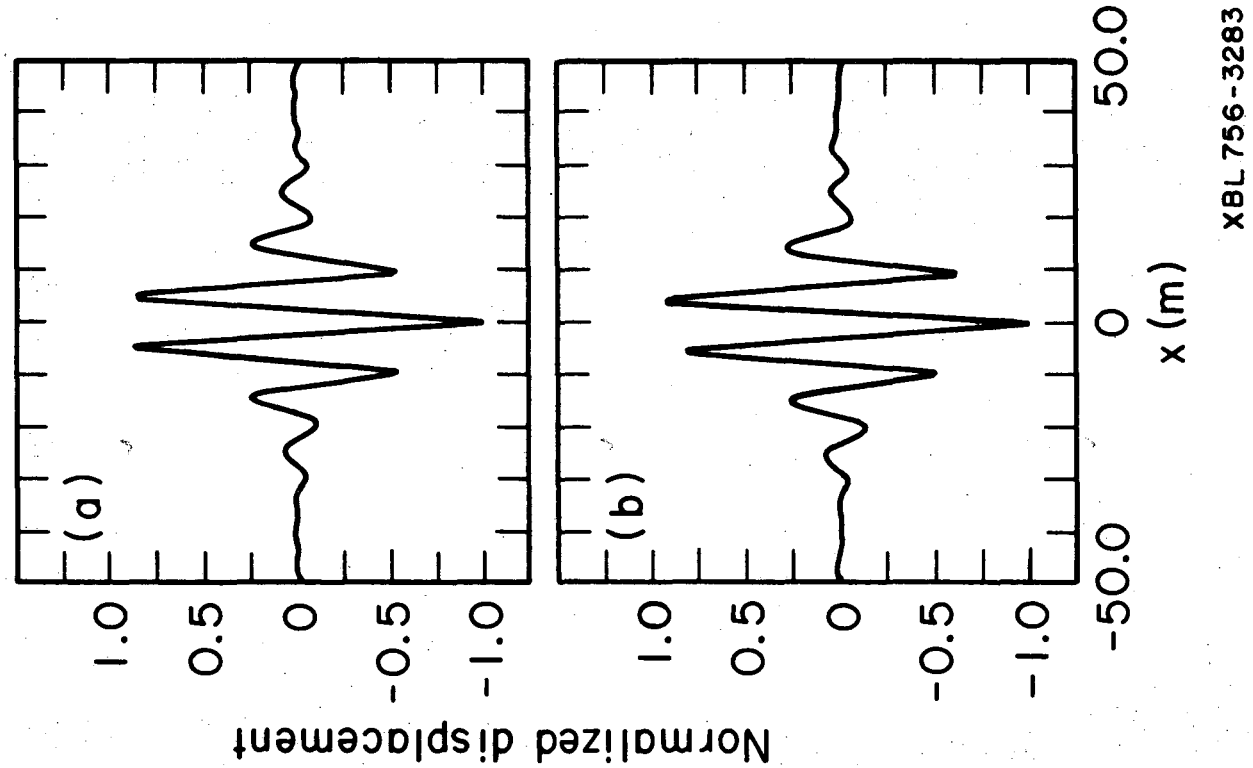

Fig. 5

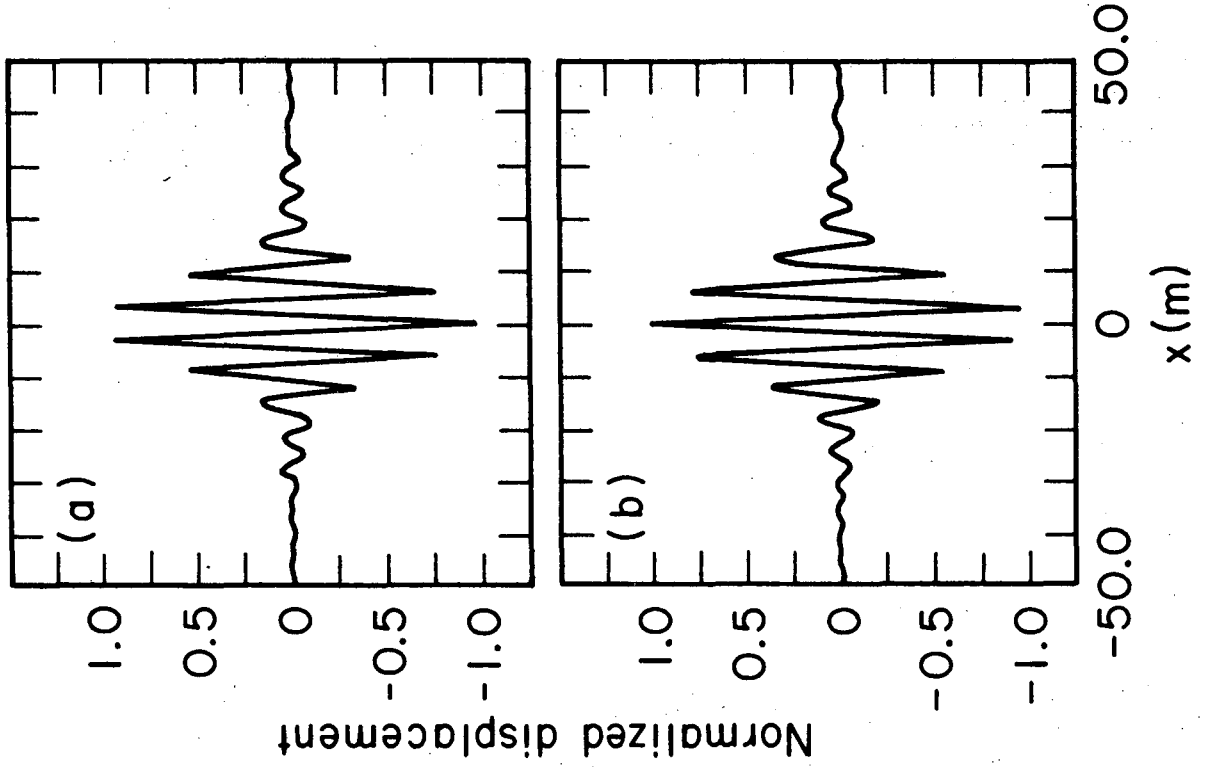

XBL756-3284

Fig. 6

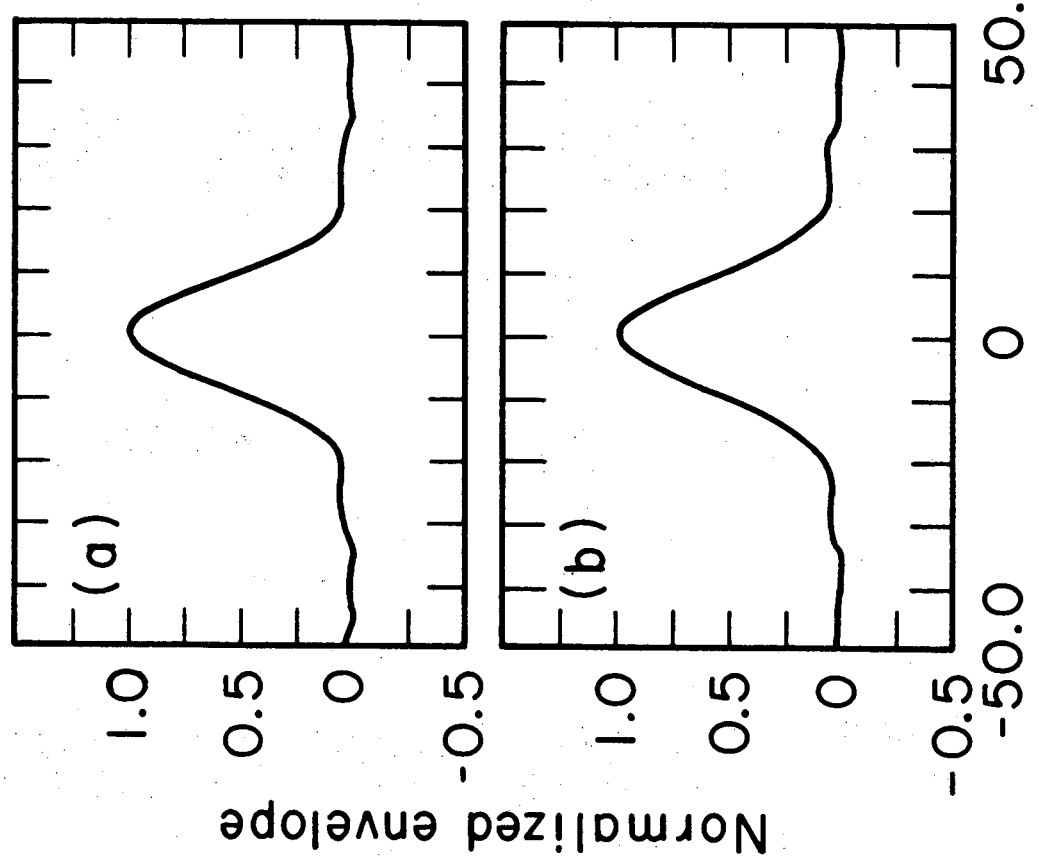

XBL756-3280

Fig. 7

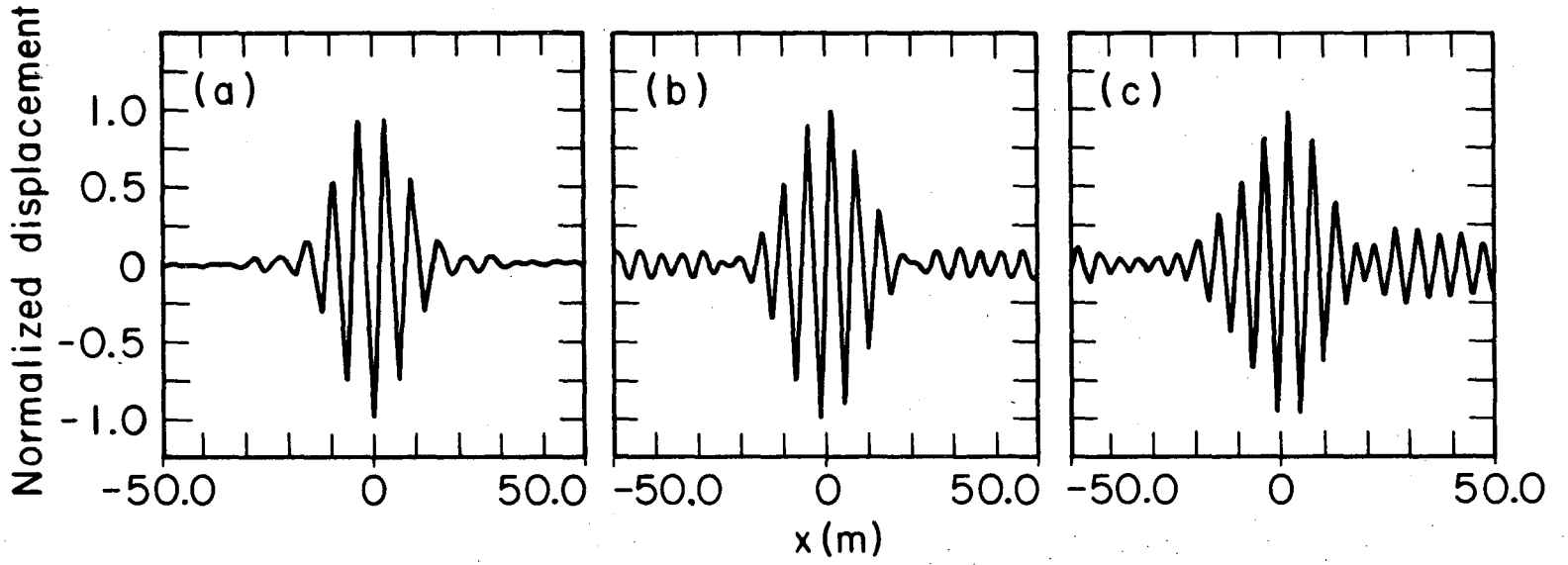
Normalized displacement
1.0
0.5
0
-0.5
-1.0
(a)
(b)
(c)
-50.0
0
50.0
x (m)
XBL 756-3285

Fig. 8

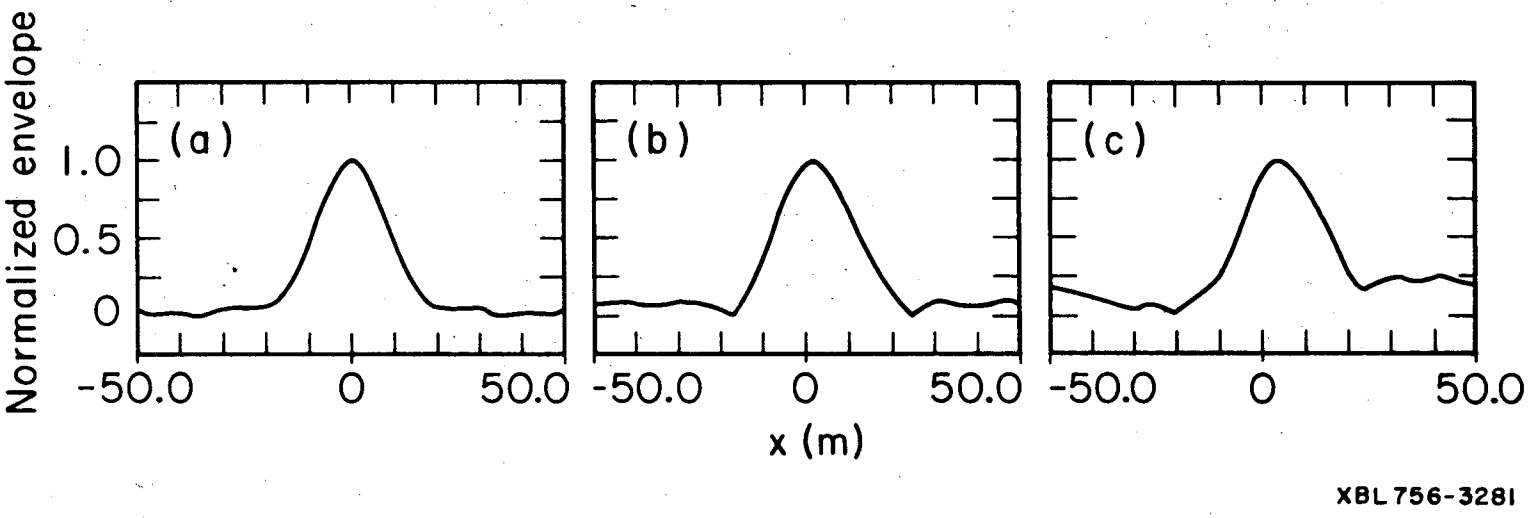

Fig. 9

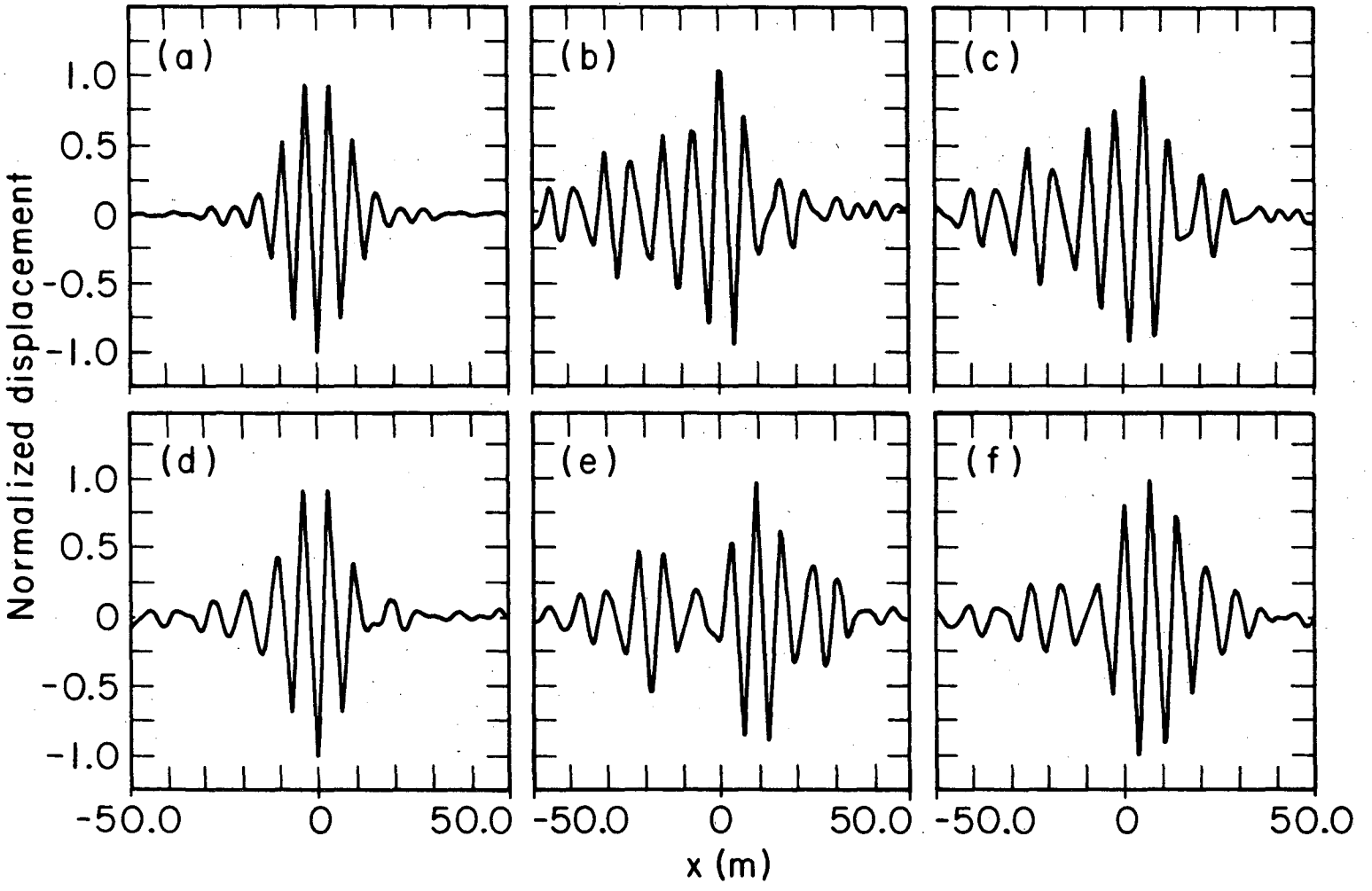
(a)
(b)
(c)
(d)
(e)
(f)
Normalized displacement
1.0
0.5
0
-0.5
-1.0
-50.0
0
50.0
x (m)
XBL756-3289

Fig. 10

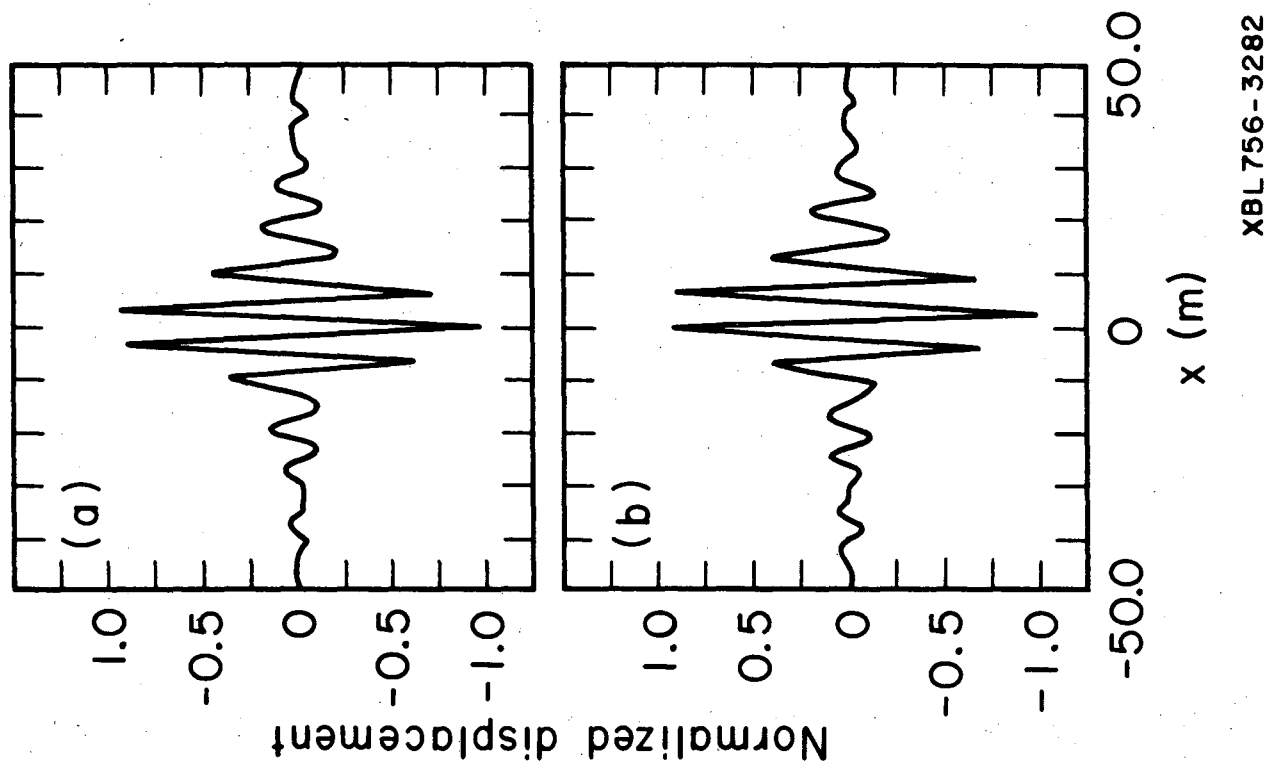

Fig. 11

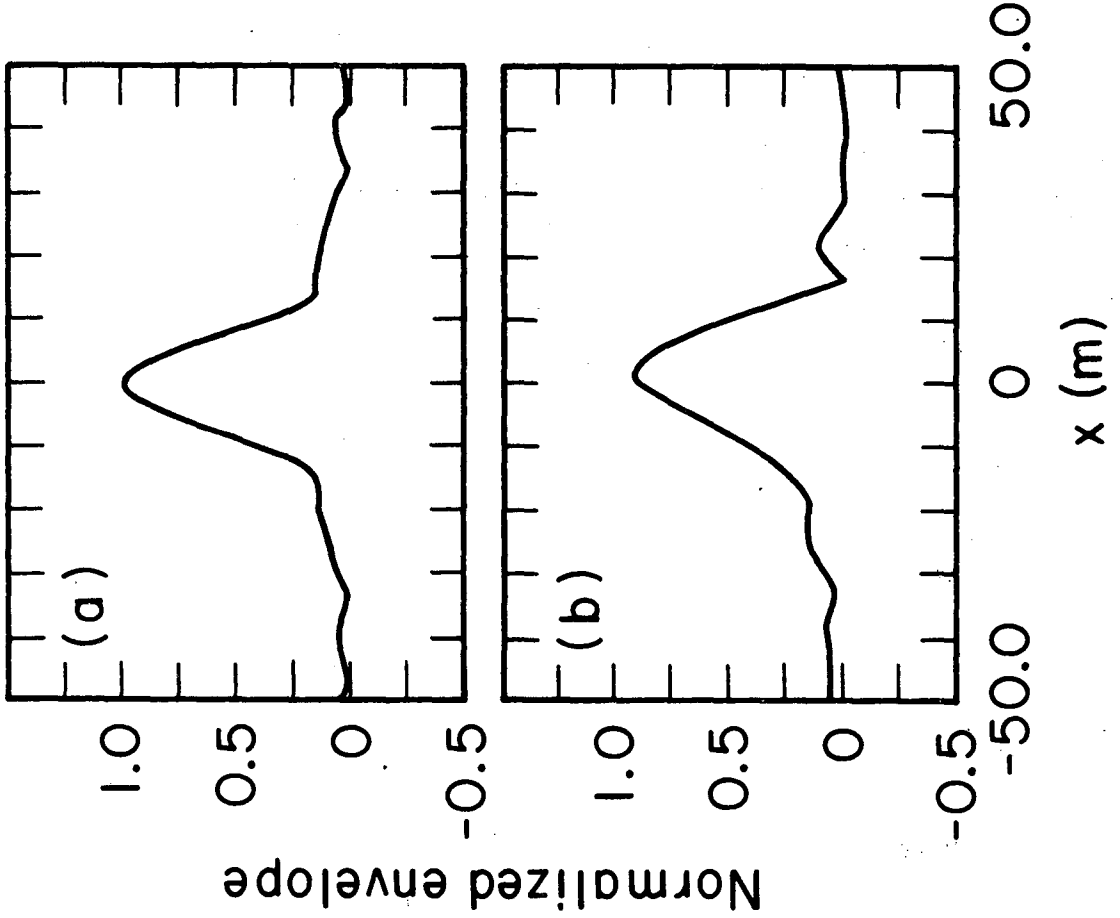

Fig. 12

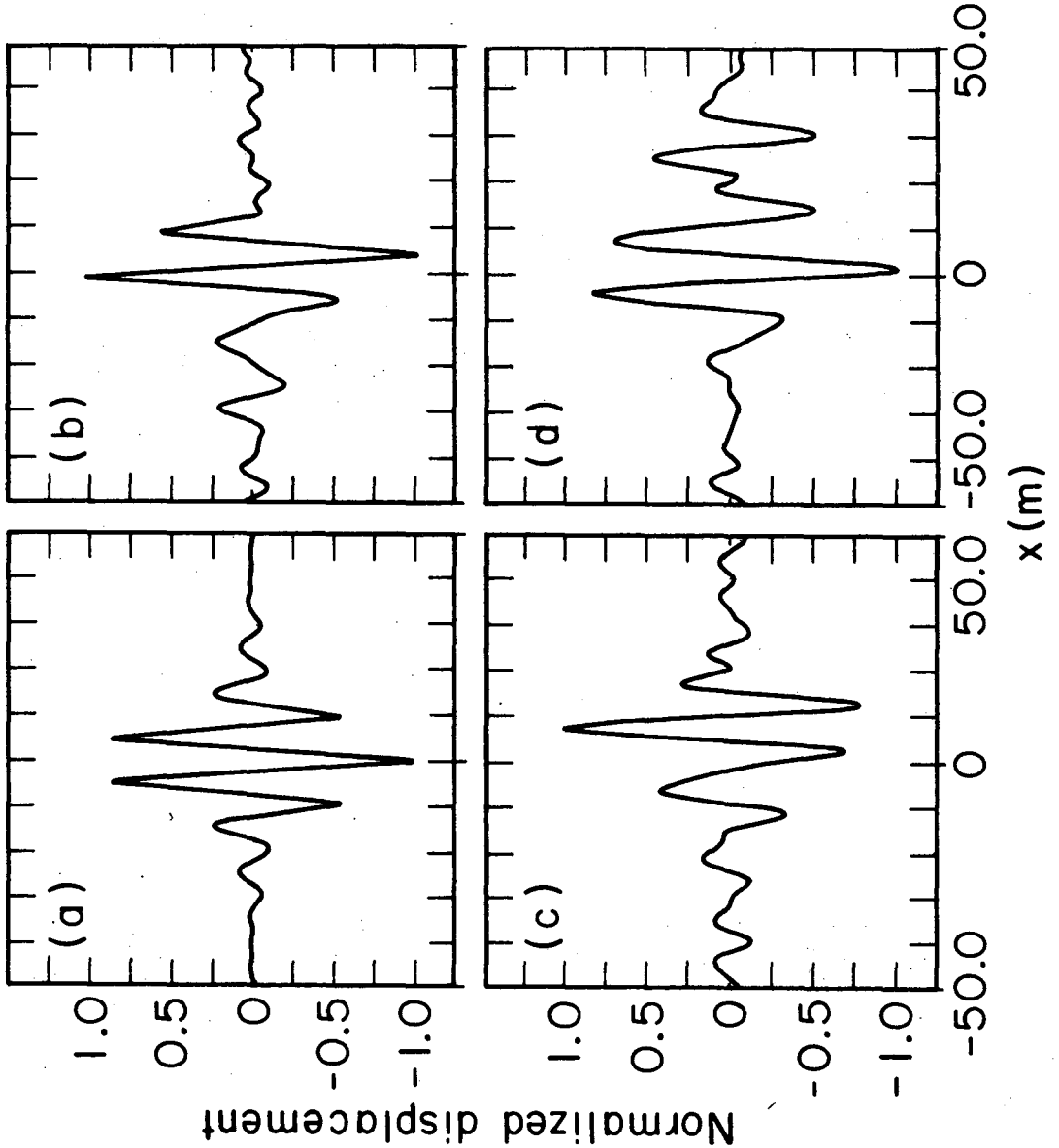
(a)
(b)
(c)
(d)
1.0
0.5
0
-0.5
-1.0
Normalized displacement
50.0
0
-50.0
x (m)
XBL 756-3288

Fig. 13

TECHNICAL INFORMATION DIVISION
LAWRENCE BERKELEY LABORATORY
UNIVERSITY OF CALIFORNIA
BERKELEY, CALIFORNIA 94720